Preparation of nanosized Bi_3NbO_7 and its visible-light photocatalytic property

Gaoke Zhang [a,*], Junling Yang [a], Shuiming Zhang [a], Qian Xiong [a], Baibiao Huang [b], Junting Wang [a], Wenqi Gong [a]

[a] School of Resources and Environmental Engineering, Wuhan University of Technology, Luoshi Road 122, Wuhan 430070, PR China
[b] State Key Laboratory of Crystal Materials, Shandong University, Jinan 250100, PR China

ABSTRACT

A nanosized Bi_3NbO_7 was synthesized by the sol–gel method. The as-prepared samples were characterized by X-ray diffraction (XRD), transmission electron microscopy (TEM), high-resolution TEM (HRTEM), UV–vis diffuse reflectance spectrum, X-ray photoelectron spectroscopy (XPS) and Brunauer–Emmet–Teller (BET). The UV–vis diffuse reflectance spectrum of the sample obtained by the sol–gel method showed a markedly blue-shift as compared to that of the sample obtained by the solid-state reaction. The band gap of the Bi_3NbO_7 nanoparticles was estimated to be about 2.43–2.59 eV. XPS analysis confirmed that the mixed valence bismuth existed in the crystal structure of the photocatalyst and niobium in the compound Bi_3NbO_7 was in the Nb^{5+} valence state. The as-prepared nanopowders exhibited a high photocatalytic activity in the decomposition of acid red G in water and acetone in air under visible-light irradiation, which may be assigned to larger specific surface area and the oxygen vacancies and mixed valence bismuth in the structure of Bi_3NbO_7.

© 2009 Elsevier B.V. All rights reserved.

1. Introduction

Photocatalysis has attracted much attention because of its potential applications in environmental purification and energy saving, it can transform solar energy into clean hydrogen energy through splitting water, and degrade harmful organic substances [1–3]. Many kinds of photocatalysis were introduced for the purpose of efficiently purifying the dye-containing wastewater, which has been considered as a cost-effective method [4–6].

TiO_2, as a semiconductor photocatalyst with large band gap (about 3.2 eV), has been intensively investigated. It can only be activated under UV irradiation ($\lambda < 388$ nm), which accounts for less than 5% of solar light energy [7–9]. From the viewpoint of using solar energy, the development of efficient visible-light-induced photocatalysts for the photodegradation of organic pollutants has been an urgent issue. Recently, complex oxide photocatalysts have been studied and showed activity for the photodegradation of organic pollutants under visible-light irradiation [10,11]. Zhang et al. reported CeO_2 for photocatalytic degradation of sulfo group-containing azo dyes in aqueous suspension irradiated by visible-light, and the results demonstrated that CeO_2 showed high photoactivity towards the degradation of azo dye [12]. Many of niobates or Bi-containing compounds, such as $K_4Nb_6O_{17}$ [13], $BiNbO_4$ [14], Bi_2MNbO_7 (M = Al^{3+}, Ga^{3+} and In^{3+}) [15], KNb_3O_8 [16],

$K_6Nb_{10.8}O_{30}$ [17] and $Bi_5Nb_3O_{15}$ [18], have also been extensively studied as a new class of photocatalysts.

In spite of its heavy metal status, bismuth is considered to be safe, as it is non-toxic and noncarcinogenic [19]. Bismuth compounds have been widely used in cosmetics and in the clinic for centuries because of their high effectiveness and low toxicity in the treatment of a variety of microbial infections, including syphilis, diarrhoea, gastritis and colitis [20]. The market for piezoceramic components is dominated by lead-based PZT materials containing more than 60 wt.% lead. Since lead is a toxic heavy metal, alkali niobates have been proposed as alternative piezoceramic materials [21]. These results show that the niobates and Bi-containing compound are non-toxic or low toxicity. However, most of niobates and bismuthides cannot effectively utilize visible radiation, and these were usually synthesized by solid-state reaction, which may result in low photocatalytic activity. Therefore, it is important to develop new niobates and Bi-containing photocatalysts with visible-light photocatalytic activity. The bismuth niobate Bi_3NbO_7 is one kind of compound with oxygen-deficient flourite structure [22] and its photocatalytic property has hardly been reported. Our study found out that it is difficult to synthesize pure Bi_3NbO_7 powders by the conventional ceramic route at high temperatures. Alternatively, attempting to synthesize nanosized Bi_3NbO_7 powders at lower temperature has been carried out by the sol–gel technique in this paper. The as-prepared nanosized Bi_3NbO_7 powders show a high photocatalytic activity for the decomposition of acid red G in water and acetone in air under visible-light irradiation.

* Corresponding author. Tel.: +86 27 87651816; fax: +86 27 87887445.
  E-mail address: gkzhang@whut.edu.cn (G. Zhang).

2. Experimental

2.1. Preparation

Bismuth(III) nitrate pentahydrate ($Bi(NO_3)_3 \cdot 5H_2O$, SCRC, China), niobium pentoxide (Nb_2O_5, SCRC, China), oxalic acid (OA, SCRC, China), citric acid (CA, SCRC, China), ethylene glycol (EG, SCRC, China), ammonia water ($NH_3 \cdot H_2O$, SCRC, China), hydrochloric acid (HCl, SCRC, China) and ethylene diamine tetraacetic acid (EDTA, SCRC, China), which were purchased from Sinopharm Chemical Reagent Co., Ltd., China, and were chosen as the initial reagents. Citric acid and ethylene glycol were used as the chelate and esterifiable reagents, respectively. All of chemicals used in the experiment were of analytical grade without further purification. Deionized water was used in the whole experiment.

A nanosized Bi_3NbO_7 with cubic structure was synthesized by the sol–gel method, the flowchart of the synthesis of Bi_3NbO_7 powders is shown in Fig. 1.

There were three steps to synthesize the Bi_3NbO_7 powders by the sol–gel method. The first step was to prepare the solution (A) containing Nb–OA, which was obtained by the hydrothermal method using the process reported in our previous study [17]. The precise concentration of niobium in the solution was determined by ICP spectrometry. The second step was to prepare the solution (B) with Bi–CA, $Bi(NO_3)_3 \cdot 5H_2O$ was added into citric acid solution, and then EDTA–ammonia solution was added slowly into the solution under unceasing stirring until $Bi(NO_3)_3 \cdot 5H_2O$ was completely dissolved. The third step was to prepare the Bi–Nb precursory solution, the solutions (A) and (B) were mixed together in the molar ratio of [Bi]:[Nb] = 3:1. The aqueous solvent in the Bi–Nb precursory solution was slowly evaporated until the formation of dark-colored, amorphous citric gels and polymeric precursors, and then kept at 450 °C for 4 h to remove the organics, then calcined at various temperatures for different times. The Bi_3NbO_7 powder synthesized by the sol–gel method is yellow in color.
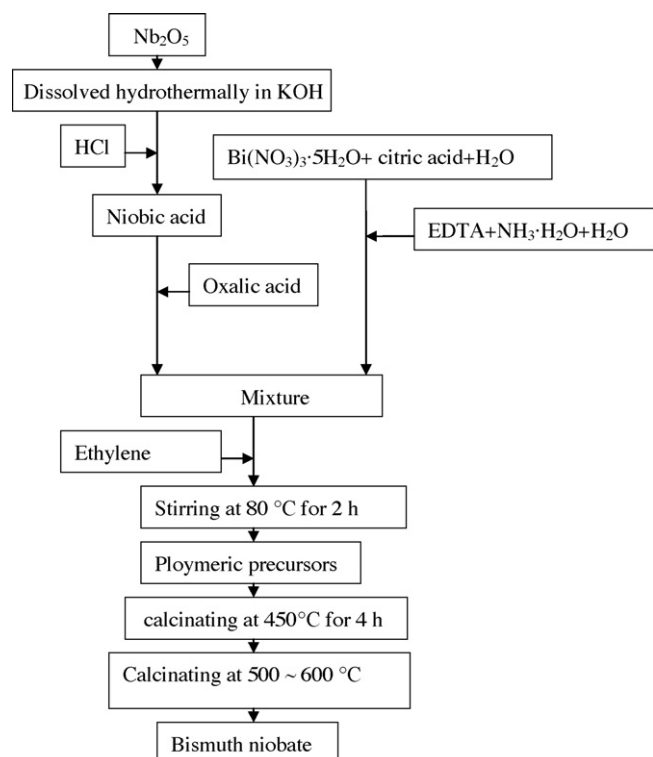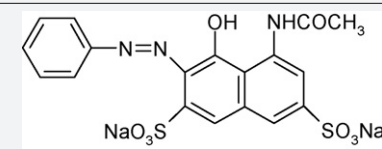

Fig. 1. Flowchart of the synthesis of Bi_3NbO_7.

λ_{max} (nm)	Molar mass (g/mol)	Structure	C.I. no.
505	509.430		18,050

The Bi_3NbO_7 powders were also prepared by the solid-state reaction at 900 °C for 2 h using Nb_2O_5 and Bi_2O_3 as raw materials.

2.2. Evaluation of photocatalytic activity

The photocatalytic activities of the as-prepared samples of Bi_3NbO_7 were evaluated by the decomposition of acid red G (Table 1) and acetone (CH_3COCH_3) under visible-light irradiation. The visible-light source was a 300 W Dy lamp with an appropriate cutoff filter (Yaguang, China). For the decolorization of acid red G, a UV cutoff filter ($\lambda = 420$ nm) was used to remove any radiation below 420 nm. 0.1 g of photocatalyst was added into 100 mL acid red G solution (50 mg/L); the pH values in all experiments were about 6.8; the distance between the liquid surface and the light source was about 20 cm, and the intensity of visible-light falling on the liquid surface was 38,000 lx measured by Digital Illuminace Meter (TES-1334A, Taiwan, ROC). Analytical samples were taken from the reaction suspensions at various time intervals during the reaction, then centrifuged the samples to remove the suspended particulates, and the concentration of acid red G was determined by measuring the absorbance at 505 nm with an UV–vis spectroscopy (UV-751GD, China). The linear relationship between the absorbance (A) at 505 nm and the concentration of acid red G (C, mg/L) can be represented empirically by the following equation: $A \approx 0.01C$. The relation between decolorization rate (X) and the absorbance (A) is given by the following equation: $X = (C_0 - C)/C_0 \approx (A_0 - A)/A_0$, where C_0 is the initial concentration of acid red G [23]. For comparison, the photocatalytic decolorization of acid red G by P25-TiO_2 and the sample obtained by solid-state reaction was also performed according to the same procedure.

For the decomposition of acetone, 0.2 g of the as-prepared photocatalyst was coating an aqueous suspension of the samples onto five dishes with diameters of 7.5 cm. The dishes containing catalysts were dried in an oven at 100 °C for about 2 h to evaporate the water and then cooled to room temperature before used. After sample-coated dishes were placed at the bottom of a gas-closed stainless steel reactor (capacity 14 L) with a glass window at room temperature, a small amount of acetone was injected into the reactor with a micro-syringe. The acetone vapor was allowed to reach adsorption equilibrium with catalysts in the reactor in the dark prior to visible-light irradiation. A UV cutoff filter ($\lambda = 400$ nm) was used to remove any radiation below 400 nm and to ensure illumination by visible-light only, and the intensity of visible-light falling on the surface of the catalyst coating was 11,700 lx measured by Digital Illuminance Meter (TES-1334A, Taiwan, ROC). The analysis of acetone and carbon dioxide concentration in the reactor was conducted online with a Photoacoustic Field Gas-Monitor (INNOVA Air Tech Instruments Model 1412, Denmark). The photocatalytic activity of the samples can be quantitatively evaluated by the decrease of acetone concentration and increase of produced CO_2 concentration.

The structure of the compound Bi_3NbO_7 was drawn by Diamond 3.1 Computer Software.

3. Results and discussion

3.1. XRD analysis

The phase composition and crystallinity of the as-prepared Bi_3NbO_7 powders were analyzed using powder X-ray diffraction (XRD) method, which was carried out on a D/MAX-RB powder X-ray diffractometer (Rigaku, Japan) with Cu Kα radiation ($\lambda = 1.54184$ Å) operated at 40 kV and 60 mA. The samples were scanned in the 2θ range of 5–70°.

The XRD patterns of the Bi_3NbO_7 powders synthesized by the sol–gel method at 500, 550 and 600 °C for 6 h are given in Fig. 2(A), respectively. The XRD patterns can be identified and indexed using the standard XRD data of Bi_3NbO_7 (JCPDS 86-0875), which crystallizes in the cubic system, space group $Fm\bar{3}m$. The six peaks in the patterns were indexed to (1 1 1), (2 0 0), (2 2 0), (3 1 1), (2 2 2) and (4 0 0) planes respectively, and can match well with the standard peaks of Bi_3NbO_7, which shows that the prepared samples consist nearly of the single phase Bi_3NbO_7 and the determined temperatures were suitable for the synthesis of the Bi_3NbO_7 powders. The XRD pattern (Fig. 2(B)) of the Bi_3NbO_7 powders synthesized by the

Table 2
Results of curve-fitting of the high-resolution XPS spectra for the Bi4f region of Bi_3NbO_7 obtained by the sol–gel method at 550 °C for 6 h.

	Bi^{3+}	Bi^{2+}
Bi4f$_{7/2}$ E_b (eV)	159.5	157.5
Bi4f$_{5/2}$ E_b (eV)	164.8	162.7
r_i (%)	93.24	6.76

solid-state reaction at 900 °C for 2 h shows that some new peaks appear besides the six peaks of Bi_3NbO_7. These new peaks could be indexed to (1 1 8), (0 0 1 6) and (2 0 1 6) planes of $Bi_5Nb_3O_{15}$ (JCPDS 39-0939), which indicates that the Bi_3NbO_7 powders synthesized by the solid-state reaction was not as pure as that prepared by the sol–gel method. It is clearly found that the width of the peaks in Fig. 2(A) is broader than that of in Fig. 2(B), which shows that the particle size of the as-prepared powders by the sol–gel method is smaller than that of the samples obtained by the solid-state reaction and could be ascribed to nanosize effect.

3.2. TEM analysis

The grain size, structure, and morphology analyses were conducted with a JEM-2100F electron microscope (JEOL, Japan), using a 200 kV accelerating voltage. Fig. 3(A) reveals the particle size of the nanosized Bi_3NbO_7 obtained by the sol–gel method at 550 °C for 6 h is about 20–40 nm. The selective area electron diffraction (SAED) pattern in Fig. 3(B) can be indexed to (3 1 1), (2 2 0), (2 0 0) and (1 1 1) planes, which indicates the particles in Fig. 4(A) were formed by aggregating some small single crystals. Fig. 3(C) shows the HRTEM image of the as-prepared Bi_3NbO_7, which indicates the size of the Bi_3NbO_7 crystal particles is less than 20 nm. The observed lattice fringe spacing of 0.31 nm corresponds to the (1 1 1) plane of the Bi_3NbO_7 crystal. This result is consistent with that of XRD patterns in Fig. 2, where the (1 1 1) peak is the strongest as compared to other patterns.

3.3. XPS analysis

The valence states of bismuth and niobium on the surface of the Bi_3NbO_7 catalyst obtained by the sol–gel method at 550 °C for 6 h were determined by X-ray photoelectron spectroscopy (XPS) in a VG Multilab 2000 system (UK) with a monochromatic Al Kα source and a charge neutralizer. The XPS survey spectrum of the as-prepared nanosized Bi_3NbO_7 is shown in Fig. 4.

High-resolution XPS spectra of Bi4f region is shown in Fig. 5, which could be fitted into four peaks 156.78, 158.61, 162.00 and 163.91 eV. The B.E. values related to the main peaks ($4f_{7/2}$) 159.5 eV and ($4f_{5/2}$) 164.8 eV and the spin-orbit splitting (5.3 eV) value are both consistent with the data of Bi_2O_3 powders [24,25], which are ascribed to Bi^{3+}. The other two peaks (157.5 and 162.7 eV) with lower energy asymmetries are evidence of a lower Bi oxidation state Bi^{2+} [26,27]. Results of curve-fitting of the high-resolution XPS spectra for the Bi4f region are shown in Table 2, r_i (%) is the ratio of each kind contribution to the total of all the bismuth contributions.

The high-resolution XPS spectra of the Nb3d region of the catalyst are showed in Fig. 6. There are two peaks 210.18 and 212.88 eV, which corresponds to the Nb3d$_{5/2}$ and Nb3d$_{3/2}$ and indicates niobium in the as-prepared Bi_3NbO_7 exists in Nb^{5+} [27,28].

3.4. UV–vis diffuse reflectance spectrum

UV–vis diffuse reflectance analysis of Bi_3NbO_7 powders was determined by UV–vis spectrometer (UV2550, Shimadzu, Japan; $BaSO_4$ was used as a reference). The UV–vis diffuse reflectance spectra of the as-prepared Bi_3NbO_7 powders obtained by the sol–gel
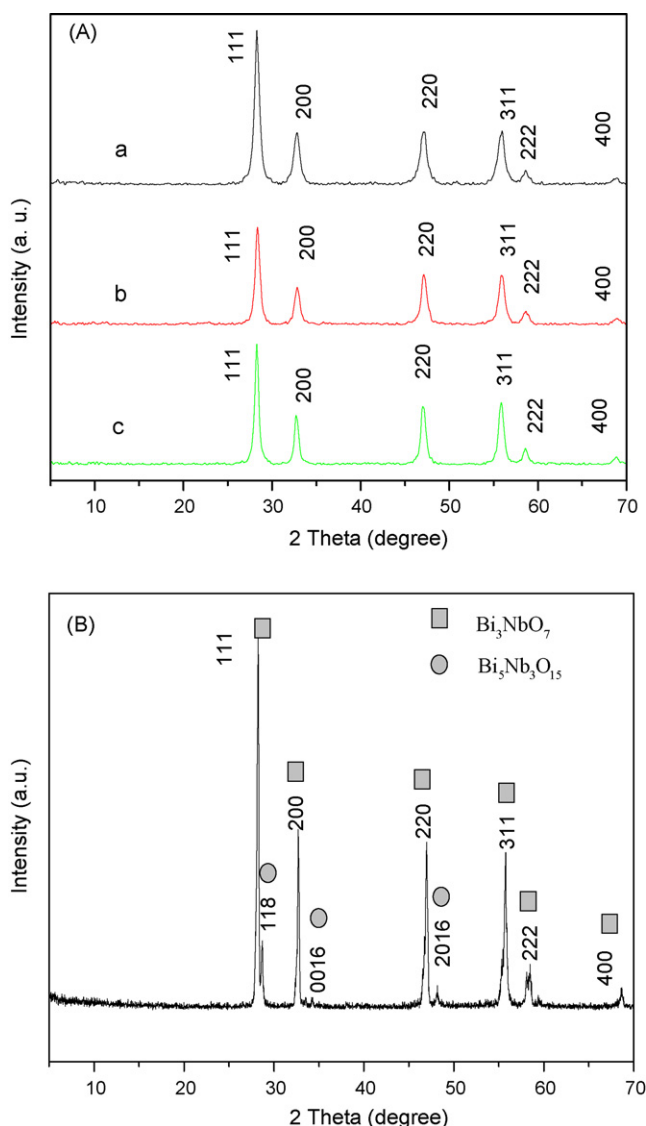

Fig. 2. Powder XRD pattern of Bi_3NbO_7 (A) prepared by the sol–gel method calcined at (a) 500 °C, (b) 550 °C and (c) 600 °C for 6 h; and (B) obtained by the solid-state method at 900 °C for 2 h.
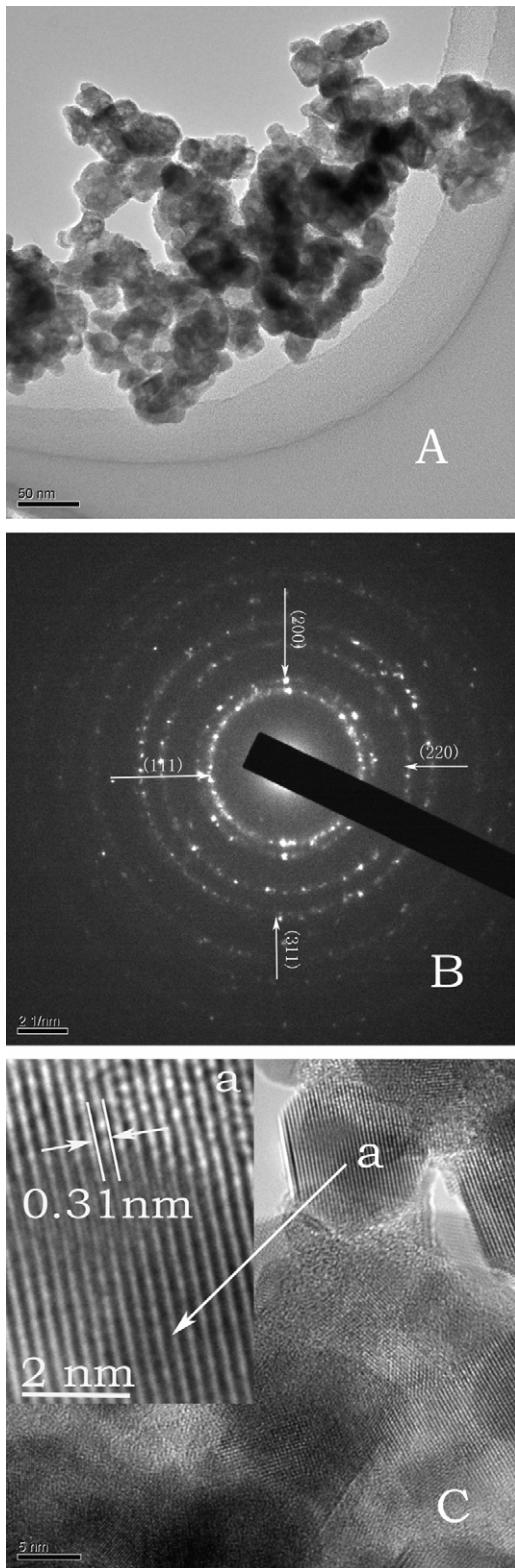
Fig. 3. TEM images of the nanosized Bi_3NbO_7 powders prepared by the sol–gel method at 550 °C for 6 h: (A) TEM image; (B) SAED pattern; (C) HRTEM image.
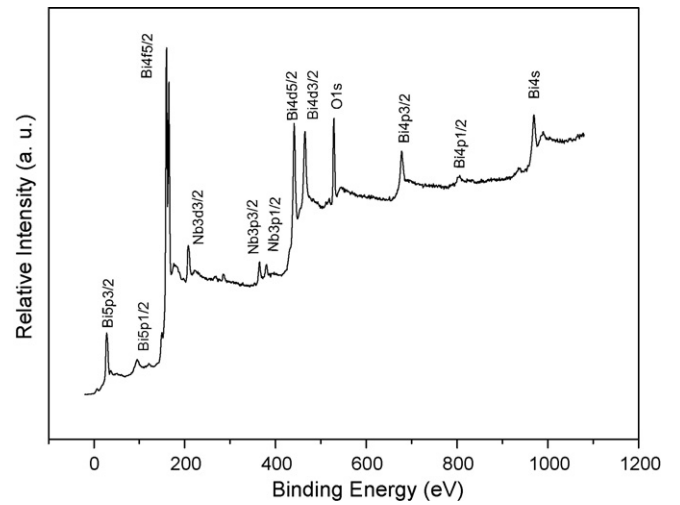

Fig. 4. XPS survey spectrum of the Nb3d region of the catalyst obtained by the sol–gel method at 550 °C for 6 h.
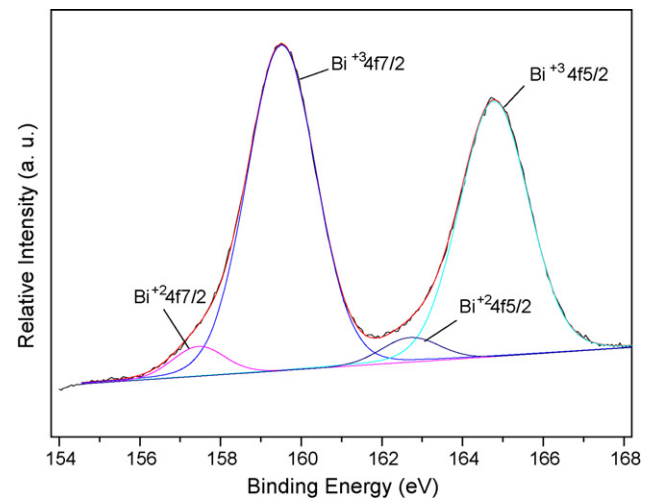

Fig. 5. High-resolution XPS spectra of Bi4f of the photocatalyst Bi_3NbO_7 obtained by the sol–gel method at 550 °C for 6 h.
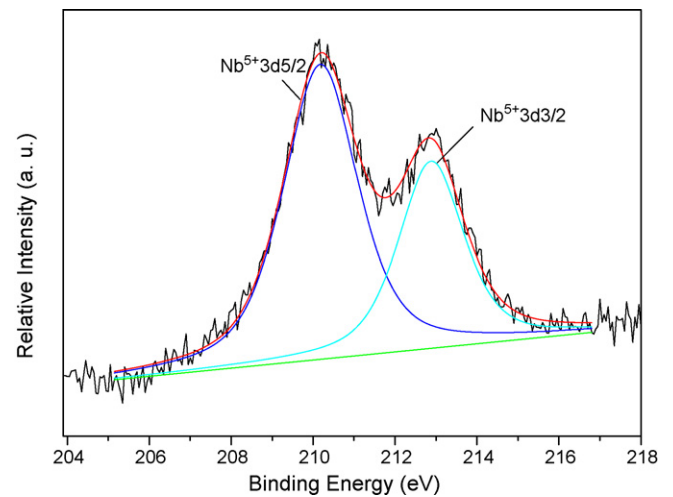

Fig. 6. High-resolution XPS spectra of the Nb3d region of the photocatalyst Bi_3NbO_7 obtained by the sol–gel method at 550 °C for 6 h.
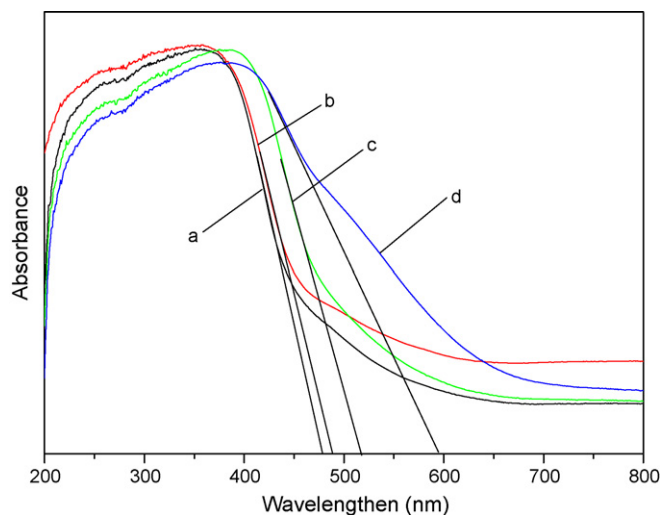
Fig. 7. UV–vis diffuse reflectance spectra of Bi_3NbO_7 powders obtained by sol–gel method calcined at (a) 450 °C, (b) 550 °C and (c) 750 °C for 6 h; and (d) by solid-state method at 900 °C for 2 h.

Fig. 8. UV–vis absorption spectra of aid red G solution (50 mg/L) during photocatalytic reaction by the catalyst (0.1 g) obtained by the sol–gel method at 550 °C for 6 h. Light intensity, 38,000 lx; pH 6.8.

method calcined at 450, 550, 750 °C for 6 h and by solid-state method calcined at 900 °C for 2 h are shown in Fig. 7. The band gap absorption edges of (a–d) are determined to be 479, 490, 511 and 598 nm [29], which correspond to the band gap energy of 2.59, 2.53, 2.43, and 2.07 eV, respectively. A significant increase in the absorption wavelength shorter than about 600 nm could be assigned to the intrinsic band gap absorption of Bi_3NbO_7. With increasing calcination temperature, the as-obtained samples show a stronger absorption in the UV–vis range and a red-shift in the band gap transition. The red-shift could be ascribed to the increase of crystal particle size. The absorption edge (Fig. 7(a)–(c)) of the catalyst Bi_3NbO_7 obtained by the sol–gel method shows a markedly blue-shift as compared to that of the sample obtained by the solid-state reaction (Fig. 7(d)). The result may be ascribed to the quantum size effect of the nanosized Bi_3NbO_7 particles obtained by the sol–gel method, which is consistent with the results of XRD and TEM analyses.

3.5. Photocatalytic activity of the photocatalysts

The photocatalytic property was evaluated by the photocatalytic decolorization of acid red G over the photocatalyst under visible-light irradiation. The changes in the absorption spectra of acid red G solution during the photocatalytic reaction process by the Bi_3NbO_7 at different irradiating times were measured by UV–vis spectrometer (UV-2102/PC, China).

UV–vis absorption spectra of acid red G (50 mg/L) in aqueous solutions during the photocatalytic reaction by the catalyst obtained by the sol–gel method at 550 °C for 6 h are shown in Fig. 8, it can be seen that there are three distinctive peaks at 215, 330 and 505 nm, which correspond to the structure of benzene ring, naphthalene ring and the nitrogen-to-nitrogen double bond, respectively. The decrease of absorption peaks of the acid red G at $\lambda_{max} = 505$ nm means that the double bond of nitrogen-to-nitrogen was destroyed. The peaks of benzene ring and naphthalene ring disappeared gradually with the increasing of reaction time, which indicated that the photocatalytic reaction also destroyed the benzene rings and the naphthalene rings.

Fig. 9(A)–(C) shows the remaining of acid red G during the photocatalytic reaction by the Bi_3NbO_7 powders prepared by the sol–gel method at 550 °C for 6 h, the solid-state reaction and P25-TiO₂ under visible-light irradiation ($\lambda > 420$ nm), respectively; while Fig. 9(D) shows the remaining of acid red G by the Bi_3NbO_7
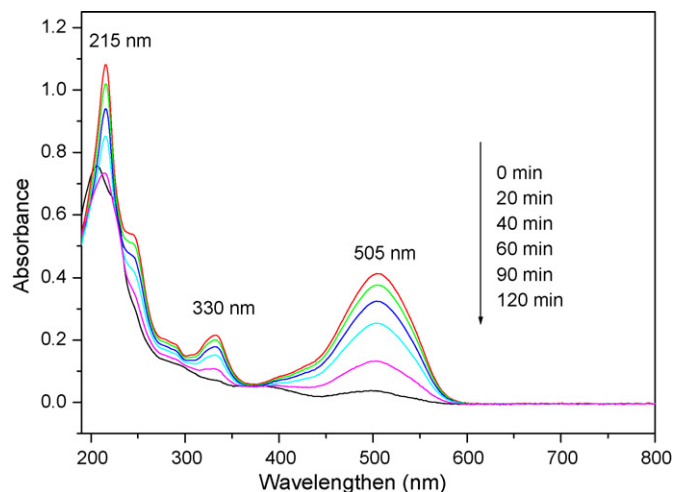
powders obtained by the sol–gel method without light irradiation. It is obvious that the decolorization rate of acid red G in the solution containing the as-prepared Bi_3NbO_7 powders is much faster than that of P25-TiO₂ and the sample obtained by the solid-state reaction under visible-light irradiation, and acid red G was hardly degraded by the catalyst obtained by the sol–gel method in darkness. From these results, it is easily found that both of visible-light irradiation and the catalysts are necessary for the efficient decolorization and the photocatalytic decolorization of acid red G solution is caused by photocatalytic oxidation reactions on the surface of the catalysts under visible-light illumination and not by the adsorption.

Fig. 10(A) and (B) shows the decolorization rates of acid red G by the Bi_3NbO_7 powders prepared by the sol–gel method at 550 °C for 6 h and the solid-state reaction, respectively. It is clearly shown that the decolorization rate of acid red G over the photocatalyst prepared by the sol–gel method (84.6%) is much larger than that of the sample synthesized by the solid-state reaction (26.44%).

To further confirm the visible-light photocatalytic properties of the as-prepared Bi_3NbO_7 nanopowders, acetone (CH_3COCH_3), which has no light absorption, was selected to evaluate the photocatalytic activity. It was found that acetone was degraded by the
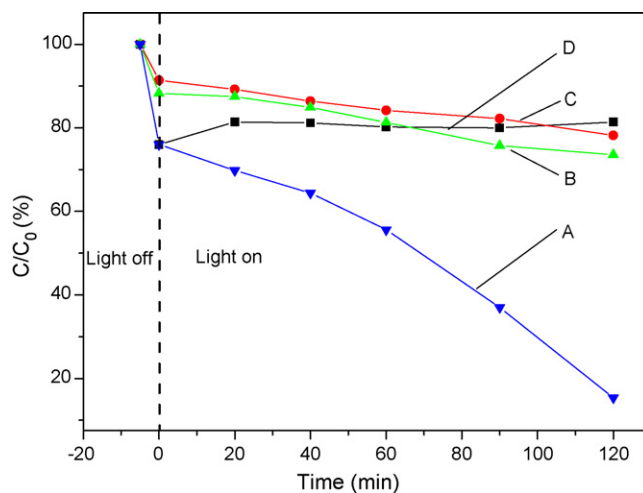

Fig. 9. The decolorization of acid red G solution (50 mg/L) by 0.1 g of (A–C) the Bi_3NbO_7 powder prepared by the sol–gel method at 550 °C for 6 h, solid-state reaction and P25-TiO₂ under visible-light irradiation; (D) the catalyst obtained by the sol–gel method without light irradiation. Light intensity, 38,000 lx; pH 6.8.
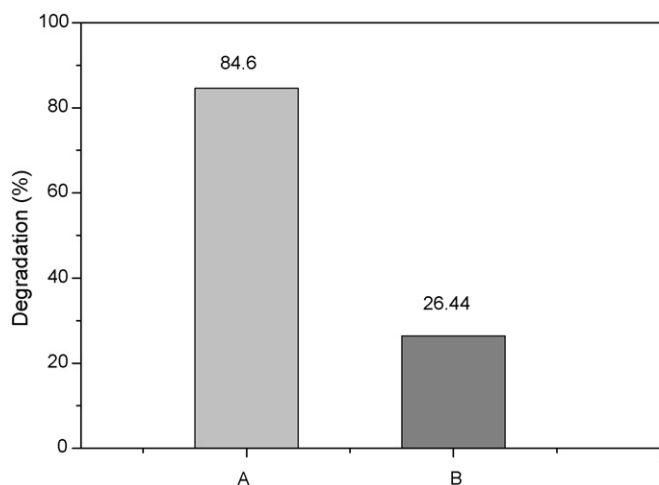
Fig. 10. The decolorization rate of acid red G (50 mg/L) over the Bi_3NbO_7 catalyst (0.1 g) obtained by (A) the sol–gel method at 550 °C for 6 h; (B) solid-state reaction. Light intensity, 38,000 lx; pH 6.8.

Fig. 12. The structure of the photocatalyst Bi_3NbO_7.

Bi_3NbO_7 nanopowders with an obvious production of CO_2 under visible-light irradiation, as shown in Fig. 11. Different from acid red G, acetone does not absorb light; thus, the photosensitization process did not exist in such a photocatalytic decomposition process. As a result, the decomposition of acetone was fully ascribed to the photocatalytic process under visible-light irradiation.

The high photocatalytic activity of the Bi_3NbO_7 photocatalyst prepared by the sol–gel method may be related to these factors. Firstly, the Bi_3NbO_7 photocatalyst prepared by the sol–gel method has a larger specific surface area, which could give more surface active sites and improve the adsorbility of the catalysts. The results of BET surface area determined by nitrogen adsorption (BelSorp-Mini system, Japan) show that the specific surface areas of the sample prepared by sol–gel method at 550 °C for 6 h is 28.07 m^2/g, which is much higher than that of the sample prepared by the solid-state reaction (0.39 m^2/g). Secondly, it may be ascribed to its special structure. It has been determined that the compound crystallizes in the cubic system (Fig. 12, drawn by Diamond 3.1 Computer Software) and exhibits a defect fluorite-type structure with 12.5% oxygen vacancies and appears a disorder in both anionic and cationic lattices. Zheng et al. reported that the presence of metallic Ag nanoparticles and oxygen vacancy on the surface of Ag/ZnO nanorods promotes the separation of photogen-
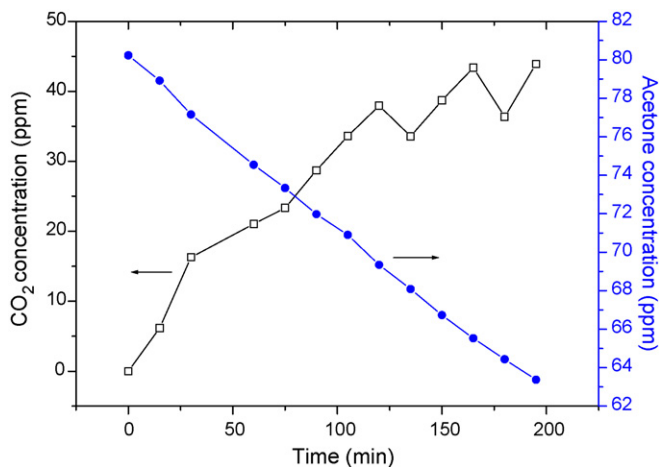
erated electron–hole pairs and thus enhances its photocatalytic activity [30]. It is thought that oxygen in the ZnO nanoflowers vacancy may act as the active centers of the catalyst, which could capture photo-induced electrons, whereas the recombination of photo-induced electrons and holes can be effectively inhibited [31]. Li et al. found that the appearance of vis photocatalytic activity for F-doped TiO_2 powders was ascribed to the creation of these oxygen vacancies [32]. Fu et al. also reported that F-doping in TiO_2 can also induce a visible photocatalytic activity by the creation of oxygen vacancies. The enhanced hydrophilicity of the as-prepared samples could also be attributed to more oxygen vacancies, which was considered to be beneficial to the photoactivity of the catalyst [33]. Therefore, during the process of photocatalytic reactions, the oxygen vacancies in the structure of Bi_3NbO_7 may become the centers to capture photo-induced electrons so that the recombination of photo-induced electrons and holes could be effectively inhibited, resulting in the higher quantum efficiency of photocatalysis. Moreover, the oxygen vacancies could promote the adsorption of O_2, and there was strong interaction between the photo-induced electrons bound by oxygen vacancies and adsorbed O_2 [34]. The activation of oxygen, especially the formation of O^{2-}, is considered to be very important for photocatalytic oxidation processes. The electron may be excited to the oxygen vacancy states from the valence band even with the energy of visible-light and the electrons excited to the oxygen vacancy state or the holes formed in the valence band perhaps react with O_2 or oxygen species and produce the reactive oxygen species such as O^{2-} or atomic oxygen [35]. Thus, the oxygen vacancies in the structure of Bi_3NbO_7 may be in favor of photocatalytic reactions in that O_2 was active to promote the oxidation of organic substances. Furthermore, the hybridization of the Bi 6s and O 2p levels makes the VB largely dispersed, which favors the mobility of photoholes in the VB and is beneficial to the oxidation reaction [36]. Moreover, the mixed valence state of bismuth in Bi_3NbO_7 may improve the mobility of photogenerated charge carriers and enhances its visible-light photocatalytic property [37,38].

4. Conclusions

The nanosized Bi_3NbO_7 with the cubic structure and oxygen vacancies was successfully prepared by the sol–gel method and its band gap energy was about 2.43–2.59 eV. The UV–vis diffuse

Fig. 11. Photocatalytic activity of the Bi_3NbO_7 nanopowders for the decomposition of acetone in air under visible-light irradiation. Light intensity, 11,700 lx.
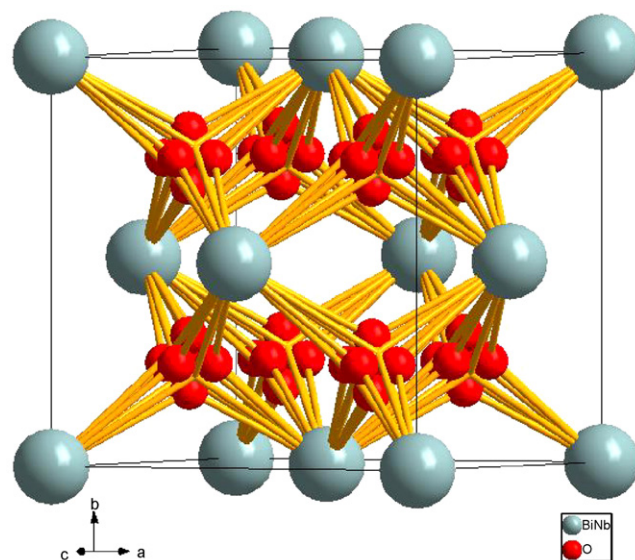
reflectance spectra of the samples obtained by the sol–gel method show a markedly blue-shift as compared to that of the sample obtained by the solid-state reaction because of the quantum size effect. The particle size of the nanosized Bi_3NbO_7 is about 20–40 nm. The mixed valence bismuth and Nb^{5+} exist in the as-obtained Bi_3NbO_7, respectively. The Bi_3NbO_7 catalysts prepared by the sol–gel method show a high photocatalytic activity for the decomposition of acid red G in water and acetone in air under visible-light irradiation. The larger specific surface area, oxygen vacancies and mixed valence bismuth in the structure of Bi_3NbO_7 may play important roles in its high visible-light photocatalytic activity.

Acknowledgements

References

[1] H.G. Kim, D.W. Hwang, J.S. Lee, An undoped, single-phase oxide photocatalyst working under visible light, J. Am. Chem. Soc. 126 (2004) 8912–8913.

[2] T. Arai, Yanagida, M. Yanagida, Konishi, Y. Konishi, Y. Iwasaki, H. Sugihara, K. Sayama, Efficient complete oxidation of acetaldehyde into CO_2 over $CuBi_2O_4/WO_3$ composite photocatalyst under visible and UV light irradiation, J. Phys. Chem. C 111 (2007) 7574–7577.

[3] J. Zhu, Ren, J. Ren, Huo, Y.N. Huo, Z.F. Bian, H.X. Li, Nanocrystalline Fe/TiO_2 visible photocatalyst with a mesoporous structure prepared via a nonhydrolytic sol–gel route, J. Phys. Chem. C 111 (2007) 18965–18969.

[4] N. Daneshvar, D. Salari, A.R. Khataee, Photocatalytic degradation of azo dye acid red 14 in water: investigation of the effect of operational parameters, J. Photochem. Photobiol. A 157 (2003) 111–116.

[5] M.R. Ghezzar, F. Abdelmalek, M. Belhadj, N. Benderdouche, A. Addou, Gliding arc plasma assisted photo-catalytic degradation of anthraquinonic acid green 25 in solution with TiO_2, Appl. Catal. B: Environ. 72 (2007) 304–313.

[6] S.F. Chen, Y.Z. Liu, Study on the photocatalytic degradation of glyphosphate by TiO_2 photocatalyst, Chemosphere 67 (2007) 1010–1017.

[7] X.T. Hong, Z.P. Wang, W.M. Cai, F. Lu, J. Zhang, Y.Z. Yang, N. Ma, Y.J. Liu, Visible-light-activated nanoparticle photocatalyst of iodine-doped titanium dioxide, Chem. Mater. 17 (2005) 1548–1552.

[8] H.Q. Sun, Y. Bai, Y.P. Cheng, W.Q. Jin, N.P. Xu, Preparation and characterization of visible-light-driven carbon–sulfur-codoped TiO_2 photocatalysts, Ind. Eng. Chem. Res. 45 (2006) 4973–4976.

[9] S.H. Kim, S.J. Hwang, W.Y. Choi, Visible light active platinum-ion-doped TiO_2 photocatalyst, J. Phys. Chem. B 109 (2005) 24260–24267.

[10] D.H. Kim, D.K. Choi, S.J. Kim, K.S. Lee, The effect of phase type on photocatalytic activity in transition metal doped TiO_2 nanoparticles, Catal. Commun. 9 (2008) 654–657.

[11] Z.Q. Yu, S.C. Steven, Chuang, The effect of Pt on the photocatalytic degradation pathway of methylene blue over TiO_2 under ambient conditions, Appl. Catal. B: Environ. 83 (2008) 277–285.

[12] P.F. Ji, J.L. Zhang, F. Chen, M. Anpo, Study of adsorption and degradation of acid orange 7 on the surface of CeO_2 under visible light irradiation, Appl. Catal. B: Environ. 85 (2009) 148–154.

[13] T. Zhong, J.L. Tang, M.K. Zhu, Y.D. Hou, H. Wang, H. Yan, Synthesis and characterization of layered niobate $K_4Nb_6O_{17}$ thin films by niobium-chelated precursor, J. Cryst. Growth 285 (2005) 201–207.

[14] B. Muktha, J. Darriet, G. Madras, T.N. Guru Row, Crystal structures and photocatalysis of the triclinic polymorphs of $BiNbO_4$ and $BiTaO_4$, J. Solid State Chem. 179 (2006) 3919–3925.

[15] Z.G. Zou, J.H. Ye, H. Arakawa, Photocatalytic water splitting into H_2 and/or O_2 under UV and visible light irradiation with a semiconductor photocatalyst, Int. J. Hydrogen Energy 28 (2003) 663–669.

[16] G.K. Zhang, F.S. He, X. Zou, J. Gong, H.B. Tu, H. Zhang, Q. Zhang, Y. Liu, Hydrothermal synthesis and photocatalytic property of KNb_3O_8 with nanometer leaf-like network, J. Alloys Compd. 427 (2007) 82–86.

[17] G.K. Zhang, Y.J. Hu, X.M. Ding, J. Zhou, J.W. Xie, Wet chemical synthesis and photocatalytic activity of potassium niobate $K_6Nb_{10.8}O_{30}$ powders, J. Solid State Chem. 181 (2008) 2133–2138.

[18] S. Tahara, A. Shimada, N. Kumada, Y. Sugahara, Characterization of $Bi_5Nb_3O_{15}$ by refinement of neutron diffraction pattern, acid treatment and reaction of the acid-treated product with n-alkylamines, J. Solid State Chem. 180 (2007) 2517–2524.

[19] N.M. Leonard, L.C. Wieland, Ram S. Mohan, Applications of bismuth (III) compounds in organic synthesis, Tetrahedron 58 (2002) 8373–8397.

[20] N. Yang, H.Z. Sun, Biocoordination chemistry of bismuth: recent advances, Coord. Chem. Rev. 251 (2007) 2354–2366.

[21] E. Ringgaard, T. Wurlitzer, Lead-free piezoceramics based on alkali niobates, J. Eur. Ceram. Soc. 25 (2005) 2701–2706.

[22] A. Castro, E. Aguado, J.M. Rojo, P. Herrero, R. Enjalbert, The new oxygen-deficient fluorite Bi_3NbO_7: synthesis, electrical behaviour and structural approach, J. Galy, Mater. Res. Bull. 33 (1998) 31–41.

[23] G.K. Zhang, X. Zou, J. Gong, F.S. He, H. Zhang, Q. Zhang, Y. Liu, X. Yang, B. Hu, Preparation and photocatalytic property of potassium niobate $K_6Nb_{10.8}O_{30}$, J. Alloys Compd. 425 (2006) 76–80.

[24] W.E. Morgan, W.J. Stec, J.R. Van Wazer, Inner-orbital binding-energy shifts of antimony and bismuth compounds, Inorg. Chem. 12 (1973) 953–955.

[25] V.S. Dharmadhikari, S.R. SainKar, S. Badrinarayan, Characterisation of thin films of bismuth oxide by X-ray photoelectron spectroscopy, J. Electron Spectrosc. Relat. Phenom. 25 (1982) 181–189.

[26] A. Gulino, S. La Delfa, I. Fragala, R.G. Egdell, Low-temperature stabilization of tetragonal zirconia by bismuth, Chem. Mater. 8 (1996) 1287–1291.

[27] K. Tabata, T. Choso, Y. Nagasawa, The topmost structure of annealed single crystal of $LiNbO_3$, Surf. Sci. 408 (1998) 137–145.

[28] V.V. Atuchin, I.E. Kalabin, V.G. Kesler, N.V. Pervukhina, Nb 3d and O 1s core levels and chemical bonding in niobates, J. Electron. Spectrosc. Relat. Phenom. 142 (2005) 129–134.

[29] J.M. Carlsson, B. Hellsing, H.S. Domingos, Theoretical investigation of the pure and Zn-doped alpha and delta phases of Bi_2O_3, Phys. Rev. B 65 (2002) 205122–205132.

[30] Y.H. Zheng, L.R. Zheng, Y.Y. Zhan, X.Y. Lin, Q. Zheng, K.M. Wei, Ag/ZnO heterostructure nanocrystals: synthesis, characterization, and photocatalysis, Inorg. Chem. 46 (2007) 6980–6986.

[31] Y.X. Wang, X.Y. Li, N. Wang, X. Quan, Y.Y. Chen, Controllable synthesis of ZnO nanoflowers and their morphology-dependent photocatalytic activities, Sep. Purif. Technol. 62 (2008) 727–732.

[32] D. Li, H. Haneda, N.K. Labhsetwar, S. Hishita, N. Ohashi, Visible-light-driven photocatalysis on fluorine-doped TiO_2 powders by the creation of surface oxygen vacancies, Chem. Phys. Lett. 401 (2005) 579–584.

[33] H.B. Fu, S.C. Zhang, T.G. Xu, Y.F. Zhu, J.M. Chen, Photocatalytic degradation of RhB by fluorinated Bi_2WO_6 and distributions of the intermediate products, Environ. Sci. Technol. 42 (2008) 2085–2091.

[34] Q. Xiao, J. Zhang, C. Xiao, X.K. Tan, Photocatalytic decolorization of methylene blue over $Zn_{1-x}Co_xO$ under visible light irradiation, Mater. Sci. Eng. B 142 (2007) 121–125.

[35] I. Nakamura, N. Negishi, S. Kutsuna, T. Ihara, S. Sugihara, K. Takeuchi, Role of oxygen vacancy in the plasma-treated TiO_2 photocatalyst with visible light activity for NO removal, J. Mol. Catal. A: Chem. 161 (2000) 205–212.

[36] A. Kudo, S. Hijii, H_2 or O_2 evolution from aqueous solutions on layered oxide photocatalysts consisting of Bi^{3+} with $6s^2$ configuration and d0 transition metal ions, Chem. Lett. 10 (1999) 1103–1104.

[37] J.W. Tang, Z.G. Zou, J.H. Ye, Efficient photocatalysis on $BaBiO_3$ driven by visible light, J. Phys. Chem. C 111 (2007) 12779–12785.

[38] N. Lakshminarasimhan, Y. Park, W. Choi, Role of valency ordering on the visible light photocatalytic activity of $BaBi^{3+}_{0.5}Bi^{5+}_{0.5}O_3$, Chem. Phys. Lett. 452 (2008) 264–268.